Proceedings of the Seventh International Conference on
Railway Technology: Research, Development and Maintenance
Edited by: J. Pombo
Civil-Comp Conferences, Volume 15, Paper 16.5
Civil-Comp Press, Edinburgh, United Kingdom, 2026
ISSN: 2753-3239, doi: 10.4203/ccc.15.16.5

Hybrid DEM-FDM Modeling of Heavy-Haul Railway Transition Zone Slope Effects on Ballast Particle Movement and Dynamic Track Responses

Y. Wang and Y. Xiao

**School of Civil Engineering, Central South University
Changsha, China**

Abstract

A two-dimensional coupled discrete element-finite difference model was developed to evaluate how transition-slope design affects the dynamic behaviour of heavy-haul ballasted bridge approaches. The ballast bed was represented with discrete particles, whereas sleepers and the underlying subgrade were modelled as continua. Field measurements from the Daqin heavy-haul railway were used to validate the coupled framework. Four inverted-trapezoid transition slopes, from 1:1 to 1:4, were then analysed. The results show that reducing the transition slope improves displacement continuity and weakens abrupt changes in sleeper, ballast, and subgrade responses at the abutment-transition and transition-subgrade interfaces. Lower slopes also reduce ballast rotation, mitigate local stress concentration, and enlarge the load-sharing region within the subgrade, whereas the influence on vertical acceleration is comparatively limited. The study clarifies both macroscopic response regularities and microscopic ballast movement in heavy-haul transition zones and provides quantitative guidance for transition design and maintenance prioritisation.

Keywords: heavy-haul railway, ballasted track, bridge transition zone, slope effects, particle movement, dynamic responses, hybrid DEM-FDM modelling

1 Introduction

Heavy-haul railways remain one of the most efficient systems for transporting bulk materials, but the increase in axle load and traffic density intensifies deterioration of ballasted bridge transition zones. Because the support stiffness changes abruptly across the abutment-transition-subgrade system, these zones are especially vulnerable to differential settlement, ballast degradation, and track irregularity [1-4].

Previous studies have shown that inverted-trapezoid transition arrangements can improve transition performance, yet the practical choice of slope still depends largely on engineering experience. Most numerical investigations have either simplified the ballast as a continuum or neglected the interaction between the ballast layer and the deformable subgrade, which limits interpretation of particle rearrangement, force-chain evolution, and local stress concentration [5-10].

To address this gap, this paper develops a coupled discrete-continuum model for a heavy-haul ballasted bridge transition zone, validates it with field measurements, and then compares four representative transition slopes. The focus is placed on the longitudinal distribution of displacement, acceleration, ballast rotation, and subgrade stress so that both structural behaviour and maintenance-sensitive locations can be identified more clearly.

2 Methods and model validation

2.1. Ballasted track bed model

The ballast bed was modelled with 7,730 Rblock particles generated according to the special-grade ballast gradation used in China[11], as shown in **Fig.1**. The computational domain was 27 m long and contained 45 sleepers. Ballast particles were generated in stages and compacted by servo-controlled loading until the final ballast thickness reached 0.55 m and the bulk density satisfied the design requirement. The principal DEM parameters in **Table 1** were calibrated from field and published data [6,12].

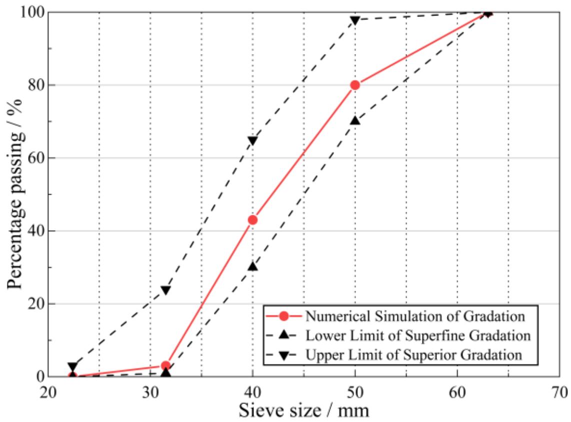

Fig. 1. Diagram of particle gradation

Parameter	Value	Unit
Ballast Particle Density	2800	kg/m^3
Ballast Particle Normal/Shear Stiffness	5.1×10^8	N/m
Ballast Particle Radius	4.1	mm
Ballast Layer Thickness	1.3	m
Sleeper Unit Density	2442	kg/m^3
Sleeper Particle Average Radius	5	mm
Sleeper Normal/Shear Stiffness	5×10^8	N/m
Friction Coefficient	0.7	-
Viscous Damping	0.25	-

Table 1. Material parameters of the ballast model[6]

2.2. Transition-subgrade models

An inverted-trapezoid transition was adopted because this form has shown favourable transition behaviour in previous studies and is widely used in practice [6-8]. Four wedge-backfill slopes, namely 1:1, 1:2, 1:3, and 1:4, were established in FLAC2D, as shown in **Fig. 2**. The subgrade was treated as an elastic continuum 27 m long and 5.5 m high, and coupling walls were placed at the ballast-subgrade interface to transfer force and velocity between the DEM and FDM domains. Free-field boundaries and Rayleigh damping were applied to suppress wave reflection and reproduce realistic energy dissipation. The main calibration parameters of the subgrade are shown in **Table 2**.

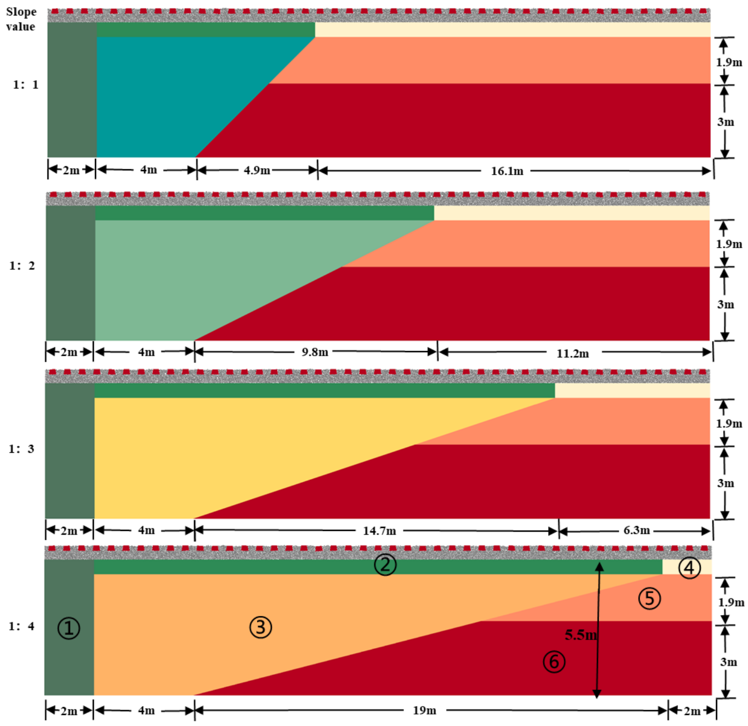

Fig. 2. Subgrade models with different slopes: ①Abutment ;② Surface layer of subgrade for transition; ③ Wedge-shaped backfill ;④ Surface layer of the subgrade; ⑤ Bottom layer of the Subgrade ;⑥ Subgrade body.

Parameter	Elastic Modulus (MPa)	Density (kg/m³)	Poisson's Ratio
Subgrade surface layer	500	1950	0.33
Subgrade bottom layer	200	1900	0.35
Subgrade body	150	1850	0.35
Wedge-shaped backfill	2500	2200	0.3
Bridge abutment	30000	24000	0.2

Table 2. Material parameters of the subgrade model[6]

2.3. DEM-FDM coupling strategy

The coupling algorithm links the vertices of the interface walls in the discrete domain to the grid nodes at the finite-difference boundary so that both domains deform synchronously. Contact forces and moments generated by the ballast particles are converted into equivalent nodal forces and transferred to the continuum, while the resulting nodal displacements drive the motion of the coupling walls and update particle-boundary contacts in the DEM region. This bidirectional exchange enables real-time interaction between ballast rearrangement and subgrade deformation throughout the train-loading process. The specific schematic diagram is shown in **Fig.3.**

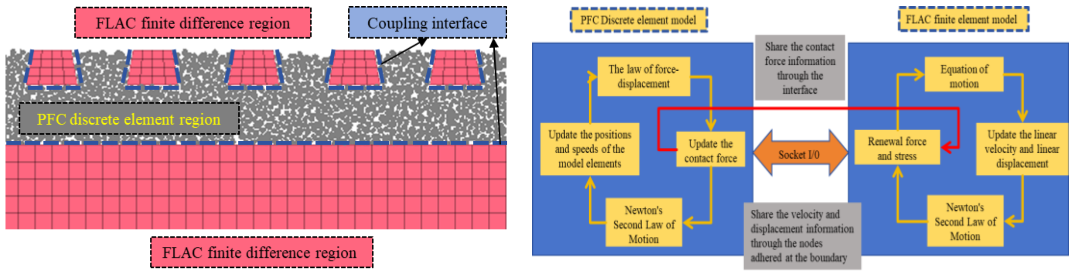

(a) Coupling interface (b) Data-exchange principle

Fig.3. Illustration of the coupling algorithm between discrete particles and continuum contact surfaces: (a) Coupling interface position; (b) Principle of Coupling Process.

2.4. Field test, loading, and validation

Field measurements were conducted at a heavy-haul bridge transition section on the Daqin railway during a maintenance window in 2021. SmartRock sensors were embedded in the ballast layer to record the local dynamic response[13,14]. In the numerical model, train loading was simplified as sequential rail-support reactions applied to successive sleepers according to axle spacing and train speed. The simulated ballast acceleration was then compared with the measured response at representative positions across the transition zone, as shown in **Fig.5**. Although the two-dimensional model slightly overestimates some vertical amplitudes, it reproduces the dominant periodicity and spatial variation observed in the field, which confirms the rationality of the coupled framework for the present parametric study.

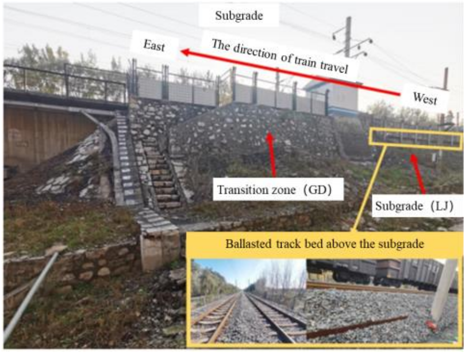

(a) Field transition section

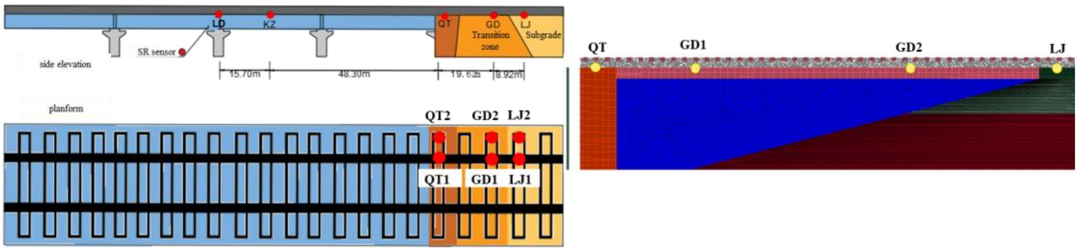

(b) Measuring point layout

Fig. 4. Field test arrangement and measurement locations.

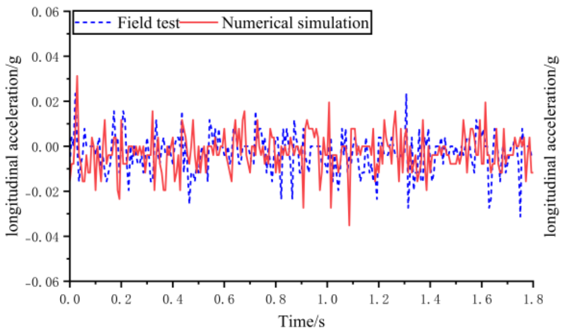

(a) Abutment section ballast (QT)

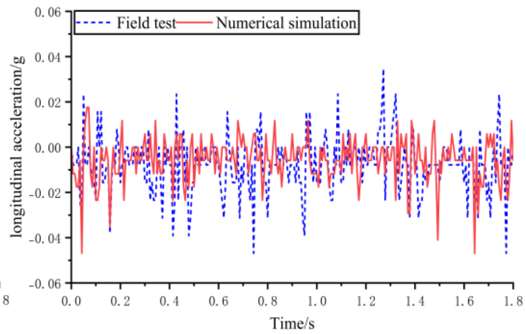

(b) Transition zone ballast 1 (GD1)

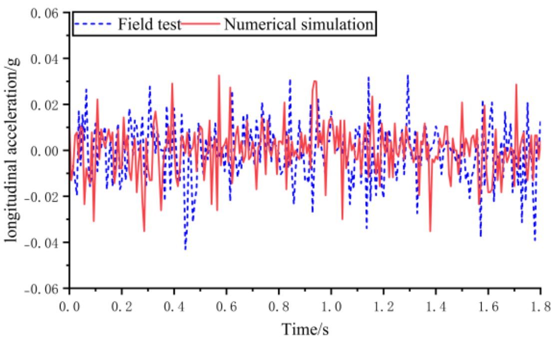

(c) Transition section ballast 2 (GD2)

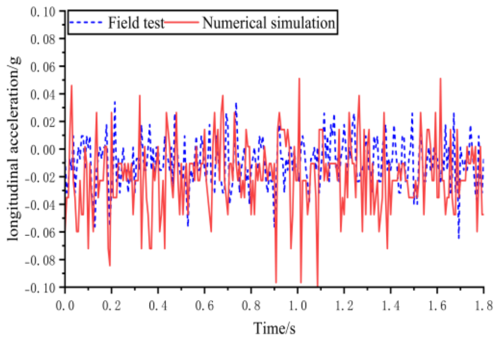

(d) Roadbed section ballast (LJ)

Fig. 5. Comparison between measurement and numerical simulation of ballast acceleration at different positions of bridge transition section

3. Results and discussion

3.1. Influence of transition slope on dynamic responses

3.1.1. Dynamic response of ballast and sleepers

Fig.6 shows the longitudinal distributions of sleeper and ballast responses under different transition slopes. The vertical displacement of sleepers rises sharply near the main stiffness-transition positions, namely around x = 10.9 m, 15.8 m, 20.7 m, and 25.0 m. A similar trend is observed for the ballast particles located 0.1 m beneath the sleepers. As the transition slope becomes gentler, the displacement transition between the abutment and the embankment becomes smoother and the peak amplitude decreases accordingly. This indicates that a smaller slope can improve structural continuity and reduce the likelihood of differential settlement at the beginning and end of the transition zone.

By contrast, the effect of slope on vertical acceleration is limited. The filtered acceleration of the sleepers remains approximately 0.02-0.03 g, while the ballast acceleration varies from about 0.014 g to 0.035 g. The ballast response is slightly larger because the monitored particles have smaller masses and experience more variable local contact conditions[15]. Therefore, slope optimisation mainly improves displacement compatibility rather than strongly altering the acceleration level.

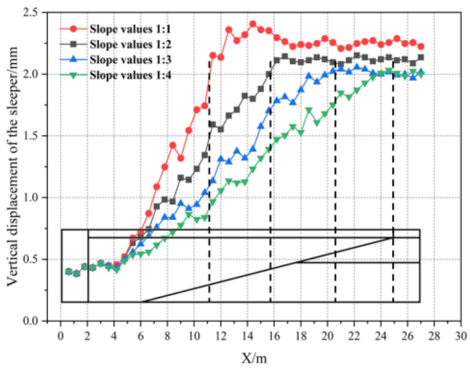

(a) Vertical displacement of sleepers

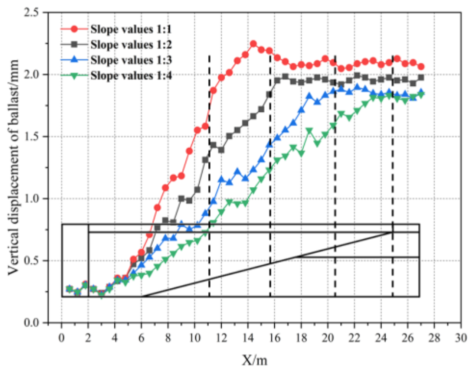

(b) Vertical displacement of ballast

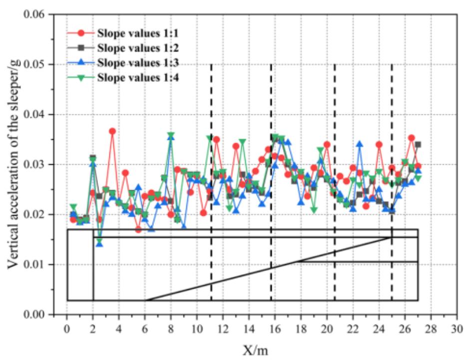

(c) Vertical acceleration of sleepers

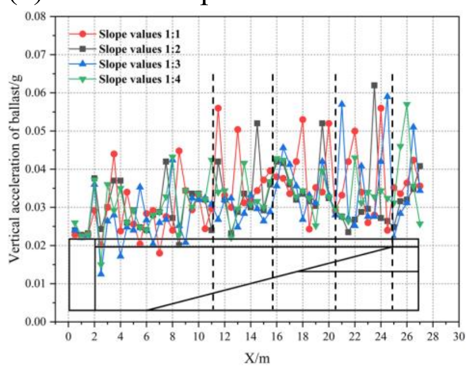

(d) Vertical acceleration of ballast

Fig.6. Dynamic response of ballast and sleepers for different transition slopes.

Ballast rotation provides additional insight into the local instability of the track bed[16,17]. As illustrated in **Fig.7**, the abutment itself exhibits relatively small particle rotation, whereas the abutment-transition interface, the wedge-backfill/subgrade interface, and the transition-subgrade interface show markedly larger cumulative rotation angles. These are exactly the zones where the support stiffness changes most strongly, indicating that abrupt stiffness variation promotes particle rolling, local rearrangement, and the risk of ballast flight or heave.

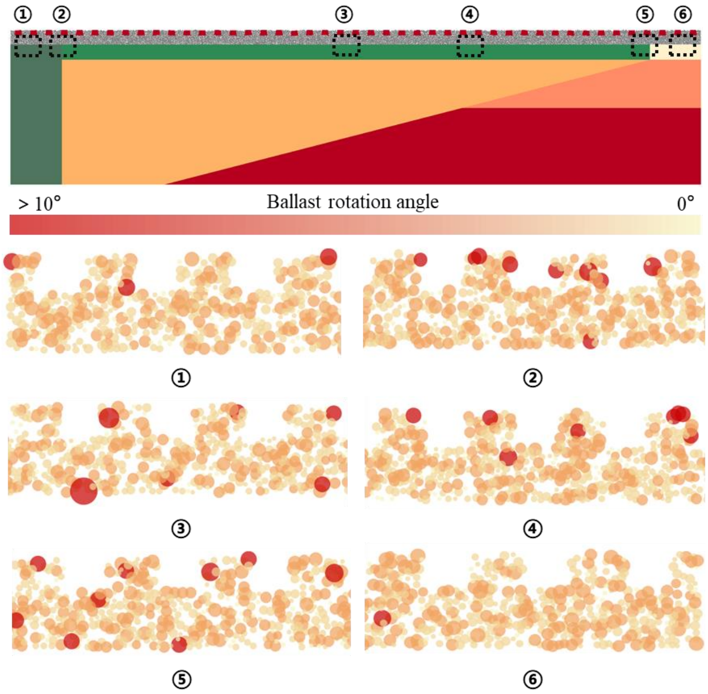

Fig.7. Distribution of ballast rotation angle in the xoz plane at representative locations.

Fig.8 further compares the rotation patterns at the transition-subgrade interface for different slopes. When the slope is reduced, both the average rotation angle and the proportion of particles rotating by more than 10 degrees decrease noticeably. This microscopic evidence is consistent with the displacement results and confirms that a gentler transition slope helps suppress local ballast disturbance and improve track-bed stability.

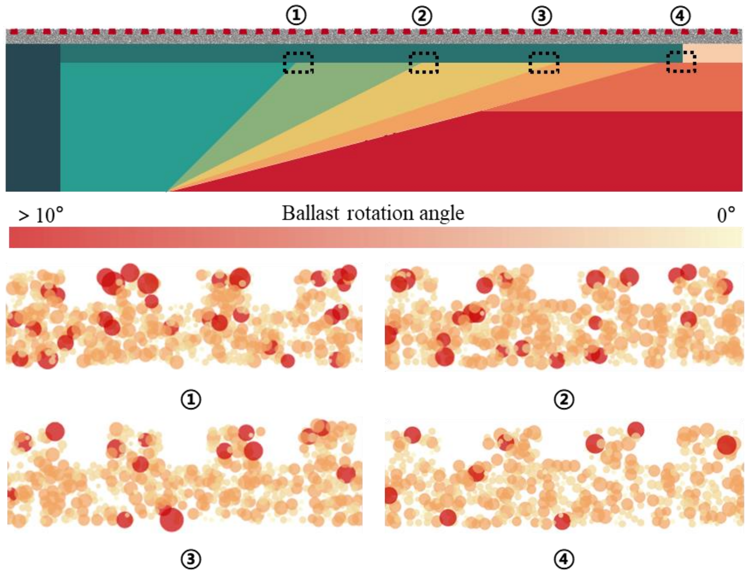

Fig.8. Ballast rotation angle at the transition-subgrade interface under different slopes.

3.1.2. Response of the subgrade surface layer

The dynamic response of the subgrade surface layer is shown in **Fig.9**. The surface displacement increases longitudinally through the transition zone, and the maximum value occurs when the wedge-backfill slope is 1:1. As the slope decreases, the overall displacement level becomes lower and the abrupt displacement jump at the backfill-subgrade connection is weakened. A similar regularity is observed for vertical stress, with the most pronounced stress fluctuation appearing near the interfaces where the support stiffness changes abruptly.

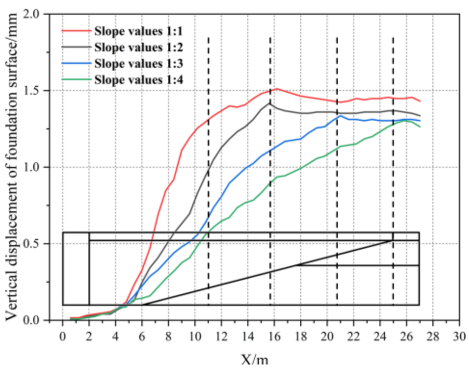

(a) Vertical displacement of the foundation surface layer

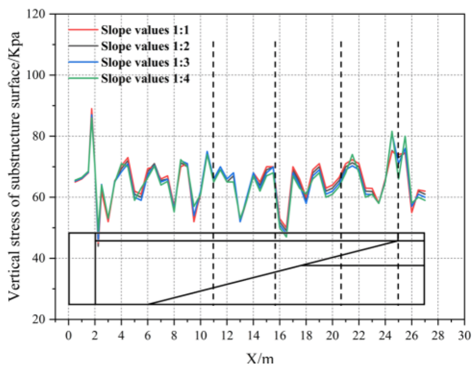

(b) Vertical stress of the foundation surface layer

Fig.9. Dynamic response of the subgrade surface layer.

Fig.10 compares the stress fields after the train passes through transition zones with different slopes. The peak stress always develops near the centre of the wedge-backfill/subgrade interface, but the distribution pattern changes considerably with the slope. For the steep 1:1 transition, the concentration zone is narrow and intense; as the slope decreases toward 1:4, the stress is redistributed over a wider area and the concentration becomes less harmful. This wider load-sharing region is beneficial for slowing the development of differential settlement in service.

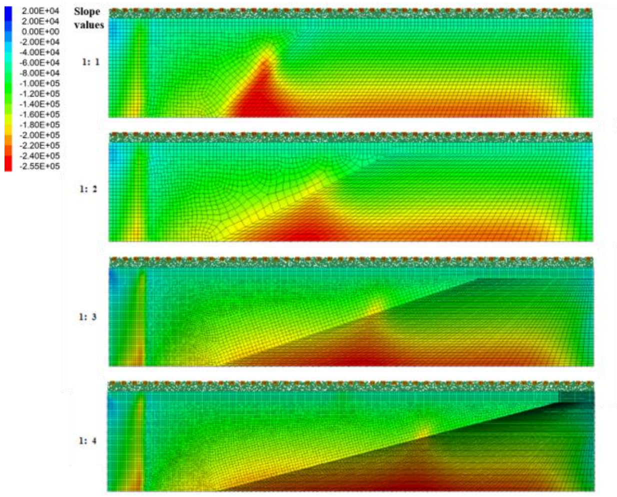

Fig.10. Stress cloud maps of the subgrade and bridge abutment for different transition slopes.

The instantaneous force-chain and stress patterns in **Fig.11** reveal how the load propagates downward from the wheelsets through the sleepers and ballast into the subgrade. The stiffness mismatch across the wedge-backfill/subgrade boundary obstructs stress transfer and produces local concentration, especially in the 1:1 case. When the slope is gentler, the interface becomes wider and the peak stress decreases, indicating that more of the subgrade participates in carrying the train load.

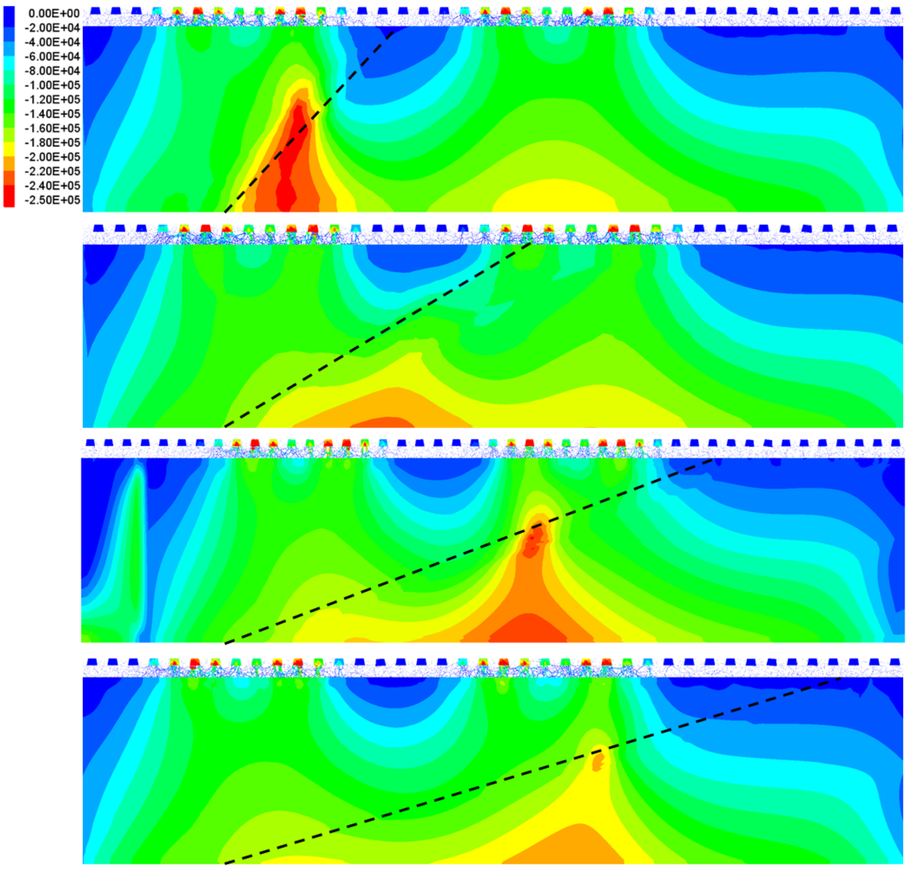

Fig.11. Ballast force-chain distribution and corresponding subgrade stress field under train loading.

Fig.12 illustrates the time-sequential stress evolution as the train moves from the transition zone toward the abutment. The high-stress region migrates with the moving load and repeatedly intensifies at the stiff-flexible boundary adjacent to the abutment. This behaviour explains why the abutment-transition interface and the transition-subgrade boundary deserve priority in inspection and maintenance planning. Overall, the combined macro- and micro-scale results consistently show that reducing the transition slope is an effective way to weaken local stress concentration, limit ballast disturbance, and improve the continuity of the heavy-haul transition zone.

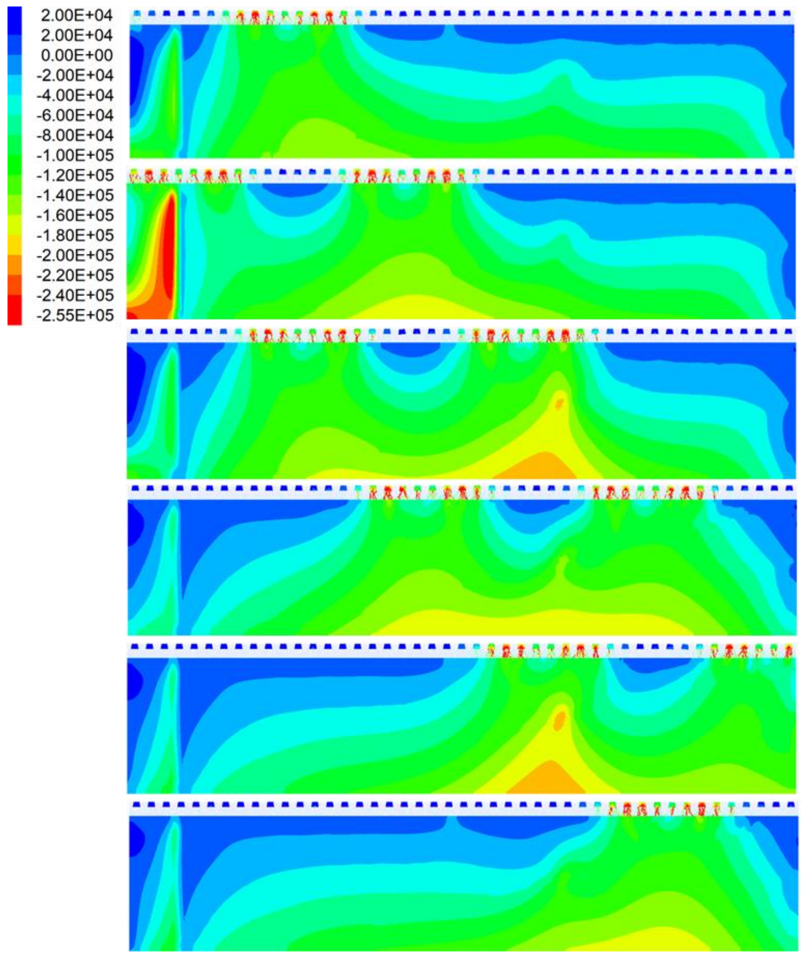

Fig.12. Time-sequential stress contour of the bridge abutment and subgrade under moving train loads.

4. Conclusions and contributions

The coupled DEM-FDM framework reproduced the dominant periodicity and spatial variation of ballast acceleration measured in the field, which supports its use for analysing heavy-haul bridge transition zones.

Transition slope mainly affects displacement compatibility rather than acceleration amplitude. A gentler slope produces a smoother longitudinal transition and reduces abrupt sleeper, ballast, and subgrade displacement changes at key stiffness-transition positions.

Particle-scale analysis shows that large ballast rotation is concentrated near the abutment-transition and transition-subgrade interfaces. Reducing the slope suppresses excessive particle rotation and therefore lowers the risk of local settlement, heave, and ballast instability.

Subgrade-scale analysis demonstrates that a smaller slope redistributes the train-induced stress over a broader region, weakens harmful stress concentration at the wedge-backfill/subgrade boundary, and provides a more favourable basis for long-term service performance and maintenance design.

Acknowledgements

Supported by China Railway Group Limited (Practical technology 2023-Special-07), the Science Fund for Distinguished Young Scholars of Hunan Province (2024JJ2073), the National Natural Science Foundation of China, and the High-Performance Computing Center of Central South University.

References

[1] H. Zhao, D. Liao, J. Gao, S. Zhu, L. Liu, J. Han, S. Li, Damage tolerance assessment of heavy-duty freight railway axles with artificial defects, Chin. J. Mech. Eng., 38, 57, 2025. DOI:10.1186/s10033-025-01218-6.

[2] A.-Q. Tian, X.-Y. Wang, H. Xu, J.-S. Pan, V. Snasel, H.-X. Lv, Multi-objective optimization model for railway heavy-haul traffic: addressing carbon emissions reduction and transport efficiency improvement, Energy, 294, 130927, 2024. DOI:10.1016/j.energy.2024.130927.

[3] T. Zhang, J. Zhou, Y. Luo, L. Zhou, Energy evolution characteristics of ballast particles and contact parameters study, Int. J. Mech. Sci., 293, 110227, 2025. DOI:10.1016/j.ijmecsci.2025.110227.

[4] H.-Z. Guo, K.-V. Yuen, H.-Q. Mu, Real-time Bayesian axle load estimation and structural identification of railway bridges under train loads based on strain monitoring, Eng. Struct., 322, 119195, 2025. DOI:10.1016/j.engstruct.2024.119195.

[5] P. Tan, Y. Xiao, Y. Jiang, M. Wang, X. Wang, C. Zhang, E. Tutumluer, Investigating influencing mechanisms of under-sleeper pads on lateral resistance of ballasted railway trackbed via hybrid DEM-FDM simulations, Transp. Geotech., 45, 101200, 2024. DOI:10.1016/j.trgeo.2024.101200.

[6] C. Shi, C. Zhao, X. Zhang, A. Andersson, Analysis on dynamic performance of different track transition forms using the discrete element/finite difference hybrid method, Comput. Struct., 230, 106187, 2020. DOI:10.1016/j.compstruc.2019.106187.

[7] P. Chumyen, D.P. Connolly, P.K. Woodward, V. Markine, A comparison of earthwork designs for railway transition zones, Constr. Build. Mater., 395, 132295, 2023. DOI:10.1016/j.conbuildmat.2023.132295.

[8] D. Nguyen, Y. Chen, A. Martinez, A DEM sensitivity study on the effects of contact parameters on triaxial response for the development of a calibration method, Comput. Geotech., 184, 107241, 2025. DOI:10.1016/j.compgeo.2025.107241.

[9] L. Li, W. Liu, M. Ma, G. Jing, W. Liu, Research on the dynamic behaviour of the railway ballast assembly subject to the low loading condition based on a tridimensional DEM-FDM coupled approach, Constr. Build. Mater., 218, 135-149, 2019. DOI:10.1016/j.conbuildmat.2019.05.102.

[10] J. Chen, J.S. Vinod, B. Indraratna, T. Ngo, Y. Liu, DEM study on the dynamic responses of a ballasted track under moving loading, Comput. Geotech., 153, 105105, 2023. DOI:10.1016/j.compgeo.2022.105105.

[11] Z. Liu, B. Feng, E. Tutumluer, Effect of ballast degradation on track dynamic behavior using discrete element modeling, Transp. Res. Rec. J. Transp. Res. Board 2676 (2022) 452–462. https://doi.org/10.1177/03611981221083921.

[12] Y. Xiao, Y. Jiang, M. Wang, W. Hua, H. Zhao, J. Mao, W. Wang, Comparative analysis on movement and vibration energy characteristics of ballast particles in heavy-haul railway transition zone, China Civil Engineering Journal, 56(9), 100-115, 2023. DOI:10.15951/j.tmgcxb.22040382.

[13] M. Palese, A.M. Zarembski, H. Huang, J. Palese, Ballast particle dynamic response as a function of subgrade support using statistical methods, Constr. Build. Mater. 325 (2022) 126772. https://doi.org/10.1016/j.conbuildmat.2022.126772.
[14] L. Fu, Z. Tian, S. Zhou, Y. Zheng, B. Wang, Characterization of ballast particle's movement associated with loading cycle, magnitude and frequency using SmartRock sensors, Granul. Matter 22 (2020). https://doi.org/10.1007/s10035-020-01029-7.
[15] Dynamic behavior analysis of high-speed railway ballast under moving vehicle loads using discrete element method, Int. J. Geomech. 17 (2017) 4016157. https://doi.org/10.1061/(ASCE)GM.1943-5622.0000871.
[16] X. Bian, W. Li, Y. Qian, E. Tutumluer, Analysing the effect of principal stress rotation on railway track settlement by discrete element method, Géotechnique 70 (2020) 803–821. https://doi.org/10.1680/jgeot.18.p.368.
[17] Characterization of ballast particle movement at mud spot | journal of materials in civil engineering | vol 31, No 1, (n.d.). https://ascelibrary.org/doi/10.1061/%28ASCE%29MT.1943-5533.0002545